

Trigonal Symmetry Breaking and its Electronic Effects in Two-Dimensional Dihalides and Trihalides

Alexandru B. Georgescu,^{1,*} Andrew J. Millis,^{2,3,†} and James M. Rondinelli^{1,‡}

¹*Department of Materials Science and Engineering,
Northwestern University, Evanston, Illinois 60208, USA*

²*Center for Computational Quantum Physics, Flatiron Institute, 162 5th Avenue, New York, NY 10010, USA*

³*Department of Physics, Columbia University, 538 West 120th Street, New York, New York 10027, USA*

(Dated: January 21, 2022)

We study the consequences of the approximately trigonal (D_{3d}) point symmetry of the transition metal (M) site in two-dimensional van der Waals MX_2 dihalides and MX_3 trihalides. The trigonal symmetry leads to a 2-2-1 orbital splitting of the transition metal d shell, which may be tuned by the interlayer distance, and changes in the ligand-ligand bond lengths. Orbital order coupled to various lower symmetry lattice modes may lift the remaining orbital degeneracies, and we explain how these may support unique electronic states using ZrI_2 and $CuCl_2$ as examples, and offer a brief overview of possible electronic configurations in this class of materials. By building and analysing Wannier models adapted to the appropriate symmetry we examine how the interplay among trigonal symmetry, electronic correlation effects, and p - d orbital charge transfer leads to insulating, orbitally polarized magnetic and/or orbital-selective Mott states. Our work establishes a rigorous framework to understand, control, and tune the electronic states in low-dimensional correlated halides. Our analysis shows that trigonal symmetry and its breaking is a key feature of the 2D halides that needs to be accounted for in search of novel electronic states in materials ranging from CrI_3 to α - $RuCl_3$.

I. INTRODUCTION

Transition metal compounds exhibit electronic properties of high scientific and technological interest, including ferroelectricity [1–4], quantum magnetism [5–10], metal-insulator transitions [11–21], and high transition-temperature superconductivity [22–26]. Transition metal oxides derived from the AMO_3 perovskite structure have been a focus of particular attention because any $3d$ or $4d$ transition metal can occupy the M site with (typically) partially filled d shells, while variation of the A-site ion can tune the relative valence of the M site ion and the electronic bandwidth. The perovskite structure is also highly polymorphic.

It allows for many variants of the basic structure that exhibit different crystallographic symmetries, which activate interesting electronic states and the pseudocubic structure allows for a wide variety of superlattices to be built [18, 19]. Basic to the electronic physics of perovskites is the cubic (O_h) point symmetry of the M-site ion and its reduction to tetragonal symmetry by even parity octahedral distortions.

Recently, two-dimensional (2D) van der Waals transition metal MX_2 dihalides and trihalides MX_3 with X a halogen ligand have become of interest as they exhibit layer-dependent ferromagnetism as in VI_3 [27–32], possible Kitaev spin liquid behavior in $RuCl_3$ [33–38] and other magnetic phenomena [39–41]. Additionally, the crystal and electronic structures are highly two dimensional, so

the materials can be exfoliated, made in monolayer form, doped by gating and layering with other compounds, and potentially twisted into Moiré materials [42]. Similar to the perovskite transition metal oxides, the M site is six-fold coordinated by ligands and can host essentially all $3d$ and $4d$ transition metals often with partial d -orbital occupancy, which endows them with the aforementioned physical properties. Dihalide and trihalide compounds with the same transition metal will exhibit different nominal valence and octahedral coordination. Table I lists structural and electronic features of several known 2D halides.

Although the sixfold coordination of the metal cations in the dihalides and trihalides would suggest octahedral symmetry O_h , analogous to the octahedral coordination in many perovskite oxides, the halides are more appropriately described as trigonally coordinated. A local orbital basis derived from e_g and t_{2g} representations of the O_h group is not the most useful description [43].

As Table I shows, the metal site symmetry in the bulk halides is either trigonal (D_{3d} , D_3 , C_{3i}) or a trigonal subgroup (C_{2h}) or even lower [44] and as previously noted for MX_2 compounds [45] a basis that conforms to the symmetry enables a more straightforward treatment of the physics.

In this paper we present a general analysis of the local electronic structure of the transition metal d shells in dihalides and trihalides, considering both ideal structures and consequences of cooperative atomic displacements. By analogy to the more frequently studied perovskite compounds, we identify what correlated electron behavior may arise. We focus on the implications of the trigonal point symmetry and answer the following questions: What is the appropriate orbital description for the correlated electrons? How to tune the orbital structure by

* alexandru.georgescu@northwestern.edu

† ajm2010@columbia.edu

‡ jrondinelli@northwestern.edu

TABLE I. Symmetry, atomic structure, d -electron configuration for the metal, and magnetic order of experimental transition metal dihalides and trihalides. AFM, FM, and HM indicate antiferromagnetic, ferromagnetic, and helimagnetic, respectively. NA and MV indicate not applicable and multiple values for the specified lengths, respectively. Structural data from Ref. [46] and magnetic data from Ref. [44].

Structure type	CdI ₂	CdCl ₂	BiI ₃	CrCl ₃	AlCl ₃
X packing	<i>hcp</i>	<i>ccp</i>	<i>hcp</i>	<i>ccp</i>	\sim <i>ccp</i>
Space group	$P\bar{3}m1$	$R\bar{3}m$	$R\bar{3}$	$P3_212$	$C2/m$
Point group	D_{3d}	D_{3d}	C_{3i}	D_3	C_{2h}
Compound	FeI ₂	NiI ₂	FeCl ₃	CrCl ₃	CrI ₃
M- d^n config.	d^6	d^8	d^5	d^3	d^3
M-site sym.	D_{3d}	D_{3d}	C_3	C_3	C_2
Magnetism	AFM	HM	HM	AFM	FM
L_1	4.050	3.927	3.380	3.483	MV
L_2	4.110	4.580	3.216	3.228	MV
L_3	N/A	N/A	3.472	3.229	MV
Compound	TiCl ₂	MnCl ₂	VCl ₃	α -RuCl ₃	α -RuCl ₃
M- d^n config.	d^2	d^5	d^2	d^5	d^5
M-site sym.	D_{3d}	D_{3d}	C_3	C_3	C_2
Magnetism	AFM	AFM, HM	AFM	AFM	-
L_1	3.430	3.711	3.471	3.44	MV
L_2	3.636	3.505	3.366	3.490	MV
L_3	NA	NA	3.366	3.487	MV

varying inter-layer distances and local MX₆ geometry, *i.e.*, ligand-ligand and metal-ligand distances? What are the consequences of symmetry reductions for the correlated electron phases.

In addressing these questions, it is often helpful to construct a Wannier basis that includes a representation of the local transition metal d orbitals, which host the electron interactions associated with correlated electron phenomena. However, standard Wannierization procedures for these materials, do not easily produce a basis that transforms properly under trigonal symmetry operations. We present a procedure for constructing an appropriate symmetry-adapted basis, which can easily be adapted to other materials. This allows us to discuss the correlated insulating states that may be obtained in stoichiometric compounds, as well as new electronic states that may appear as a result of further symmetry breaking, such as those present in the semi-1D chains in ZrI₂, and certain polymorphs of RuCl₃, CrI₃ and other halides [44].

II. LOCAL STRUCTURE: ELECTRONIC STATES AND SYMMETRY CONSIDERATIONS

The basic structural unit of 2D halides is a plane of transition metal ions, with each transition metal ion coordinated with 6 halogen ions (Figure 1A). Unlike in the layered perovskite-based transition metal compounds, the local axes of the octahedron surrounding a transition metal ion in a halide are rotated with respect to the

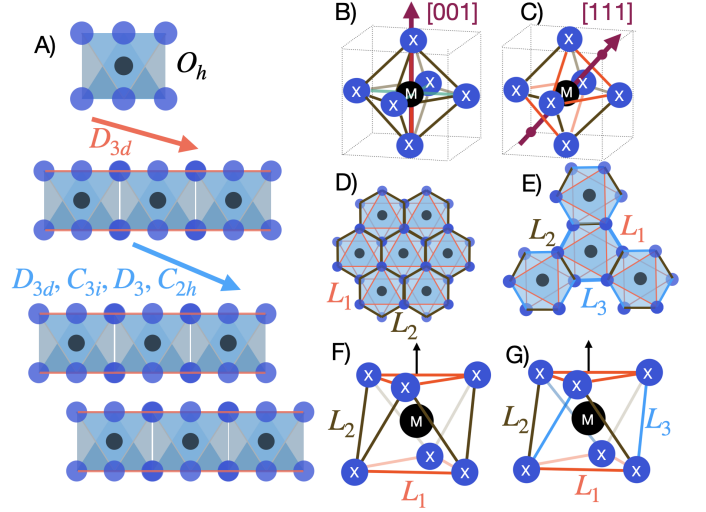


FIG. 1. A) Sequential illustration of symmetry breaking as a result of the layered structure in dihalides and trihalides. Placing an ideal octahedron within a monolayer will reduce its O_h symmetry to trigonal D_{3d} symmetry: 3-fold rotations along the z axis are preserved, and so is mirror and inversion symmetry - even without distortions to the octahedron itself. Sketch of B) tetragonal and C) trigonal symmetry breaking of an octahedron. Heavy magenta arrows indicate vector normal to monolayer planes. Layer structure of MX₆ octahedra for D) MX₂ dihalides and E) MX₃ trihalides. Definitions for halide-halide lengths for octahedra in F) MX₂ and G) MX₃ halides. The red edges with length L_1 surround the face parallel to the monolayer planes, L_2 are edges that are not parallel to the material plane and that connect nearest-neighbor MX₆ octahedra. L_3 edges do not connect octahedra, are not parallel to the plane, and only appear in MX₃ compounds.

axes that define the two-dimensional plane. Specifically, choosing coordinates such that the monolayer plane is perpendicular to [001] then the octahedral axes (M-X bond directions) are $[\pm 1 \pm 1 \pm 1]$ in the ideal halides (compare panels B and C of Figure 1). In the ideal monolayer case, the point symmetry of the M ion is then D_{3d} . The symmetry may be further reduced by spin-orbit coupling, additional relaxations of the atomic positions, magnetic order and by different stackings of the layered structures. We discuss some lattice symmetry reductions, as well as magnetic order later.

The key feature of the D_{3d} symmetry is a three-fold rotation axis, in the ideal case perpendicular to the monolayer plane of MX₆ octahedra (Figure 1D,E) and passing through a triangular X₃ face (Figure 1F,G).

In D_{3d} symmetry, the M-X bond lengths remain equal, however, the X-X ligand distances L_i ($i = 1 - 3$) need not be equal. The inequivalence is accommodated through changes in the X-M-X intra-octahedral angles. Similar effects are known in edge sharing perovskites [47, 48]. Because of the planar structure formed by edge connectivity of the octahedra, the halogen-halogen distances perpendicular to (001) (denoted L_1 in panels F and G

TABLE II. Relationships among the atomic d orbitals for the standard cubic (tetragonal) basis with z aligned to the (001) direction shown in Figure 1B and trigonal basis with z axis aligned to (111) direction shown in Figure 1C. Note that in the absence of trigonal symmetry breaking, the a_{1g} and e_g^σ orbitals become degenerate and combine to transform as the t_{2g} representation.

Cubic Basis [001]		Trigonal Basis [111]	
Symmetry	Orbitals	Symmetry	Orbitals
t_{2g}	$d_{\bar{x}\bar{y}}$	a_{1g}	d_{z^2}
	$d_{\bar{y}\bar{z}}$	e_g^π	$\frac{2}{\sqrt{6}}d_{xy} + \frac{2}{\sqrt{3}}d_{yz}$
	$d_{\bar{x}\bar{z}}$		$\frac{2}{\sqrt{6}}d_{x^2-y^2} - \frac{1}{\sqrt{3}}d_{xz}$
e_g	$d_{\bar{x}^2-\bar{y}^2}$	e_g^σ	$\frac{1}{\sqrt{3}}d_{x^2-y^2} + \frac{2}{\sqrt{6}}d_{xz}$
	$d_{\bar{z}^2-r^2}$		$\frac{1}{\sqrt{3}}d_{xy} - \frac{2}{\sqrt{6}}d_{yz}$

of Figure 1) are inequivalent to X-X distances on other triangular faces.

This can be plainly observed in the MX_2 compounds, where X-X edges not parallel to the plane connect different octahedra, while those that are parallel to the plane connect the same octahedra. This leads to the inequivalence of the L_1 and L_2 X-X edges (Figure 1F).

One may parametrize the trigonal distortion away from perfect octahedral coordination either by the L_2/L_1 ratio or by the X-M-X bond angles. We find that the L_2/L_1 ratio is a more convenient parametrization in D_{3d} symmetry, as it plays an analogous role to the c/a ratio for the tetragonal symmetry and tunes the splitting between the doublet and singlet.

For the MX_3 compounds only half of the X-X edges not parallel to the plane connect MX_6 octahedra, leading to a total of three inequivalent edges, L_1 , L_2 , and L_3 . Figure 1D illustrates that in both cases, there are only two types of inequivalent faces: those parallel to the planes of MX_6 , with three L_1 edges, and those oblique to the plane with edges L_1 , L_2 and L_3 .

While the symmetry of an ideal halide monolayer is D_{3d} , different arrangements of the planes can lead to symmetry reductions to D_3 or C_{3i} in the bulk compounds (see Table I). These subgroups, however, lead to the same trigonal orbital basis for the transition metal d orbitals. Further, anisotropic semicovalent and van der Waals interactions or additional electronically driven orderings can lead to further symmetry reductions (see Table I). In such cases the clearest way to understand the resulting orbital structure is as an additional symmetry reduction beyond trigonal.

The trigonal symmetry has implications for the electronic structure. Under D_{3d} symmetry, the 5 d orbitals transform as two doublets (e_g^σ and e_g^π) and a singlet (a_{1g}). The wave functions and level splittings are not constrained by symmetry and depend on details of atomic-scale physics. The trigonal structure of the halides may be viewed as a weak distortion of the O_h symmetry familiar from cubic perovskites, enabling a simpler interpretation

of the basis functions. Under O_h symmetry, the atomic d orbitals transform as an e_g symmetry doublet (wavefunctions conventionally chosen as $d_{\bar{x}^2-\bar{y}^2}$ and $d_{3\bar{z}^2-r^2}$) and a t_{2g} triplet (wavefunctions conventionally chosen as $d_{\bar{x}\bar{y}}$, $d_{\bar{x}\bar{z}}$, $d_{\bar{y}\bar{z}}$) where \bar{x} , \bar{y} , \bar{z} are the three octahedral axes. Ligand fields arising from hybridization lead to an energy separation between the doublet and triplet states of the order of 2 eV. The further reduction of the symmetry from O_h to D_{3d} does not additionally split the e_g states, which now form the e_g^σ doublet representation of D_{3d} . It does, however, split the t_{2g} triplet into an e_g^π doublet and an a_{1g} singlet with the $e_g^\pi - a_{1g}$ level splitting being typically smaller than the energetic separation to the e_g^σ doublet. Then to first order in the trigonal distortion, the basis functions for the e_g^σ representation are linear combinations of the familiar cubic-basis e_g states while the basis functions for the e_g^π and a_{1g} states are linear combinations of the familiar t_{2g} states. (Table II) [49]. Lowering the symmetry below trigonal, in particular by breaking the C_3 rotational symmetry about the axis perpendicular to the plane, will lift the degeneracies of the two e_g doublets. Such distortions may occur if the transition metal valence is such that one of the orbital pairs forming a doublet are partially filled, enabling an electronic symmetry-breaking transition.

III. PHYSICS OF THE TRIGONAL DISTORTION IN TiCl_2

We now present density functional theory (DFT) calculations on the representative dihalide TiCl_2 [50], using the experimental structure obtained from ICSD [46]. TiCl_2 exhibits a d^2 electronic configuration and its primitive $P\bar{3}m1$ structure contains a single formula unit. The Ti atoms are aligned along z , making for the simplest possible stacking. The Ti site symmetry is D_{3d} . Details of its crystal structure are presented in Table I.

We begin by analyzing non-magnetic DFT calculations using the PBE functional, in order to isolate the effect of the atomic structure on the on-site crystal field splittings and orbital order before performing further analysis. We then investigate correlation effects in the DFT+U approximation. This stepwise approach allows us to disentangle the effects of the structure from that of d -shell electron-electron interactions. We select different inter-layer distances, X-X distances, and L_2/L_1 ratios to probe the trigonal symmetry effects on the orbital structure. We characterize the electronic structure changes via the on-site energy of the orbitals at the Γ point, and the orbital occupations, as obtained from the eigenvalues of the density matrix defined from orbital projectors.

Experimentally, these perturbations to the inter-layer distance may be realized via external pressure, while the L_2/L_1 ratio can be tuned via epitaxial strain. The effects we find pertain to MX_3 compounds as well, as the MX_3 structure can be obtained from the MX_2 structure by removing 1/3 of the M atoms and keeping the ligand

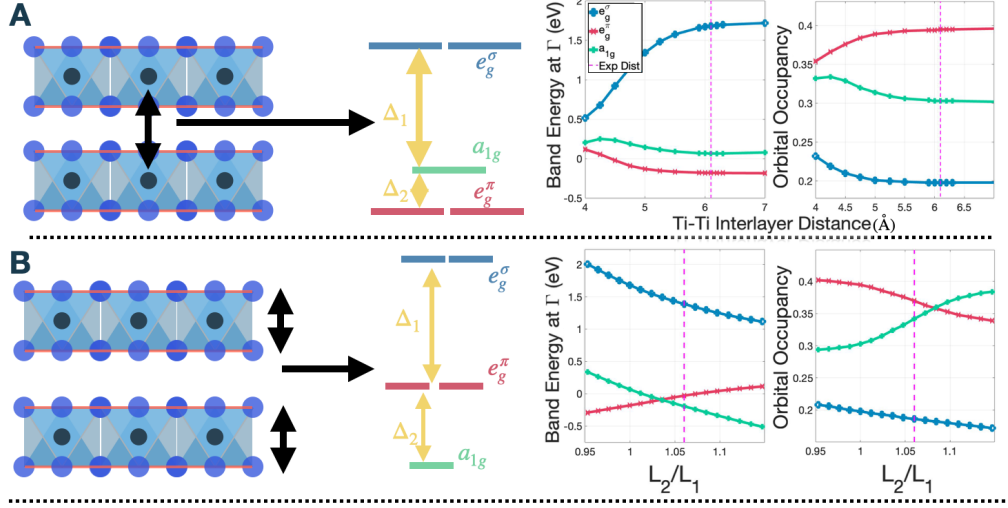


FIG. 2. Electronic orbital splitting at the non-magnetic DFT level for TiCl_2 as a function of (A) Ti-Ti interlayer distance and (B) L_2/L_1 ratio, as quantified by crystal field splitting at the Γ point and orbital occupancy as obtained from the density matrix of the orbital projections. In A, the octahedron is kept perfect, with a X-X distance of 3.43 Å. In B, the inter-layer distance is kept fixed to the experimental value, while L_2/L_1 is varied. The experimental inter-layer distance and L_2/L_1 ratio are indicated with broken magenta lines.

octahedral structure intact.

A. Level Splittings and Orbital Occupancies

Figure 2 presents a summary of our results.

Starting with the experimental structure, we find that the energy splitting at Γ corresponds to the expected 2-2-1 orbital splitting as shown by the vertical broken line in Figure 2A,B.

Upon visualizing isosurfaces of the wavefunctions in real space at the Γ point (not shown), we find the orbitals represent wavefunctions of the trigonal basis.

These wavefunctions are similar to the Wannier functions presented in Figure 3.

The lowest energy Ti d -derived state at Γ is the a_{1g} state. The wavefunction exhibits lobes directed through the faces parallel to the plane. The next two higher energy states are the e_g^π doublet with wavefunction lobes directed at the faces of the octahedron transverse to the plane. The highest energy states transform as the e_g^σ doublet in which the orbital lobes are directed along the octahedral axes, pointing towards the Cl anions. This behavior is expected because they behave equivalently to the e_g states of the cubic basis. The e_g^σ - e_g^π splitting of approximately 1.5 eV is somewhat less than the approximately 2–3 eV splitting typical in perovskite transition metal oxides, reflecting the larger energy separation and weaker hybridization of the metal d states with the halogen ligand p -states.

Next, we examine the effects on the electronic structure of varying the structural parameters (Figure 2). We begin by fixing the TiCl_6 octahedra to $L_1 = L_2 = 3.430$ Å with all M-X bonds fixed to 2.425 Å and vary the inter-

layer distance. We find that the crystal-field splitting between the e_g^σ and the e_g^π/a_{1g} complex increases with increased inter-layer distance as does the corresponding difference in orbital occupancy (Figure 2A). The $e_g^\pi - a_{1g}$ splitting is less dependent on the interlayer distance. For inter-layer distances greater than or equal to the experimental value measured at ambient pressure, the crystal field splitting and orbital occupations converge to their asymptotic isolated layer values.

Next, we keep the inter-layer distance fixed to the ambient pressure equilibrium experimental value of 6.1 Å and vary the L_2/L_1 ratio by displacing the Cl atoms along z . This changes L_2 while keeping L_1 the same. We find that increasing L_2 increases the energy difference between the highest two and lowest three orbital states. In contrast to the effect of increasing the inter-layer distance, changing L_2/L_1 also decreases the a_{1g} orbital energy relative to the e_g^π energy. The occupancies change in the corresponding manner. The relative sizes of the energies and the orbital splittings, however, are not fixed. Importantly, we find that the critical L_2/L_1 ratio at which the occupations are equal occurs at a different critical L_2/L_1 ratio that gives a vanishing energy difference for $e_g^\pi - a_{1g}$ orbitals. Both correspond to $L_2/L_1 \neq 0$, underlining that the symmetry of the representation of the Ti d -shell is always at most trigonal, and never cubic.

B. Orbital Physics in the Trigonal Wannier Basis

Key to understanding the physical effects in a correlated material is an appropriate tight-binding model, which can be constructed via a Wannierization procedure

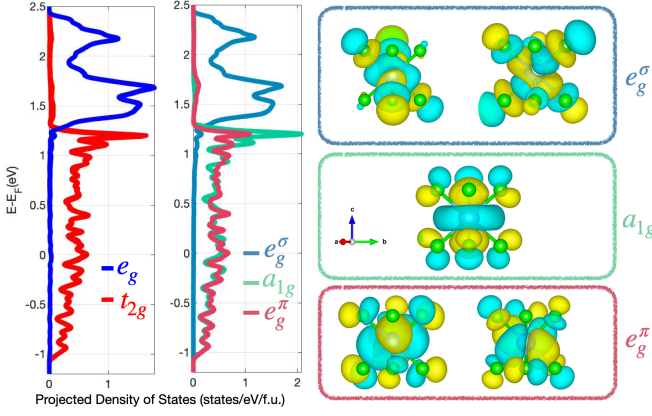


FIG. 3. Projected density of states for the Wannier functions for TiCl_2 in the tetragonal basis (left) and trigonal basis (center). Eigenstates of the density matrix, as obtained by diagonalizing the density matrix (right).

as implemented in standard electronic structure codes. A Wannierization is in effect a choice of a basis that represents band states in a certain energy range, along with a projection of the density functional Hamiltonian onto this basis. It is desirable to choose a basis that is adapted to the physics of the problem at hand; both because an appropriate choice provides physical insight and because the form and magnitude of beyond-DFT interactions depends on the basis chosen.

Standard application of the Wannier90 [51] code to di- and trihalide compounds tends to lead to the e_g - t_{2g} basis functions well adapted to O_h symmetry. To obtain Wannier functions adapted to trigonal symmetry, we find it is best to first use Wannier90 to obtain a basis, and then rotate the basis to obtain a diagonal density matrix. Another option is to diagonalize the Wannier Hamiltonian at the Γ -point. A third choice is to diagonalize the on-site term in the real-space Wannier Hamiltonian. To obtain real-space isosurfaces, we used the eigenvectors obtained by diagonalizing the density matrix to build a linear superposition of the Wannier functions obtained directly from Wannier90.

Figure 3 shows the density of states projected onto different combinations of the Wannier states obtained for TiCl_2 in a standard application of Wannier90 (left panel) and in the basis that diagonalizes the density matrix (center panel) after the rotation. The total density of states is the same in both cases. The e_g^σ -derived states, which are derived from the same functions in both cases, are approximately the same. The trigonal functions allow us to distinguish the higher-lying a_{1g} states from the lower-lying e_g^π states. Figure 3 also shows the corresponding isosurfaces of the resulting Wannier functions, which we obtain through linear mixing.

We now analyze the resulting Hamiltonian $H_{\vec{R}_i}$ (Figure 4), where the rows (columns) correspond to the following d orbitals: the first two correspond to e_g^σ , the middle one to a_{1g} and the last two to e_g^π . For $\vec{R} = (0, 0, 0)$, we

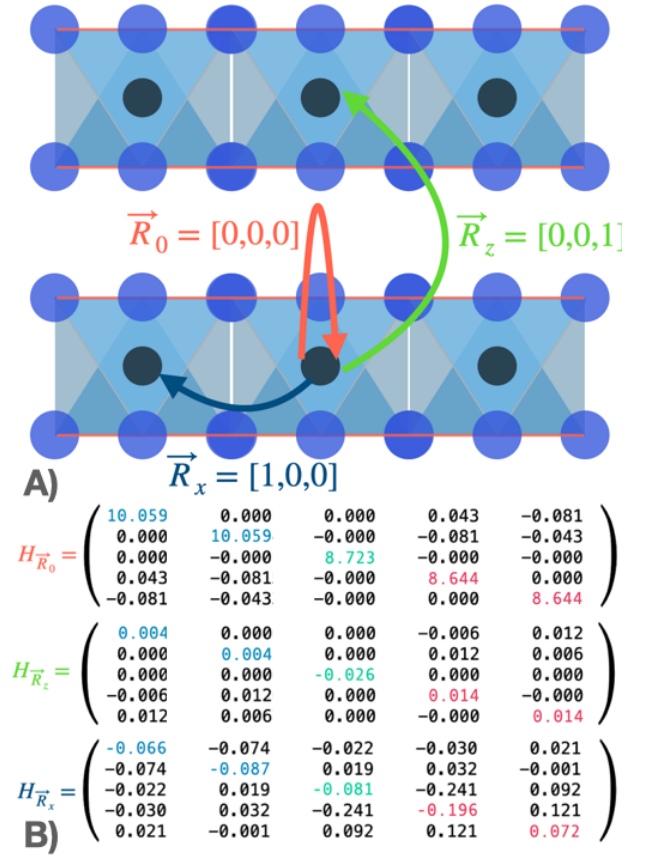


FIG. 4. A) \vec{R} connecting transition metals M, for which we show the hopping matrices of the Hamiltonian below in B). The diagonal elements are shown in blue for e_g^σ , a_{1g} in green, and e_g^π red.

find that the a_{1g} orbital is orthogonal to the other sets of orbitals in $H_{\vec{R}_0}$, similar to what is obtained in the atomic orbital projection matrix. While within the pairs of degenerate doublets the mixing is practically 0, there is however mixing between the two pairs. This $H_{\vec{R}_0}$ however possesses the 2-2-1 pattern of eigenvalues consistent with D_{3d} symmetry. Hopping along z between the Ti atoms $\vec{R} = (0, 0, c)$ is primarily driven by a_{1g} - a_{1g} hopping, hopping between the two pairs of doublet states, as well as small but non-zero hopping between equivalent orbitals as gleaned from $H_{\vec{R}_z}$ in Figure 4B. Finally, hopping in-plane between the atoms $\vec{R} = (a, 0, 0)$ is driven by non-zero hoppings between all orbitals, however the lowest three orbitals in $H_{\vec{R}_x}$ are the largest, as expected from the spatial orientation of the orbital lobes discussed previously. We also note that one of the eigenvalues of the hopping Hamiltonian is close to 0. The zero eigenvalue pertains to hopping among the highest two energy (e_g^σ) orbitals. As a result, there will always be a weakly dispersing flat band among the higher e_g states along high symmetry directions in the zone.

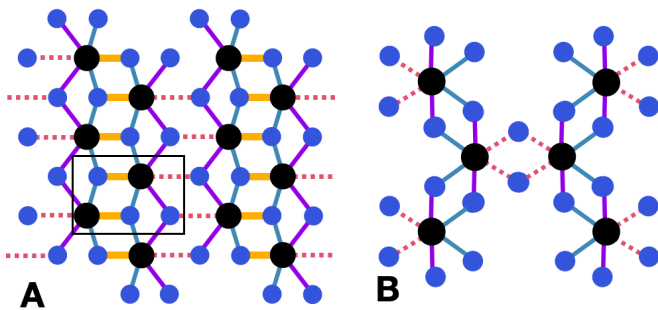


FIG. 5. Single layer lattice structure for materials with point group symmetry C_{2h} , which breaks the degeneracy of the doublets: A) a layer of MX_2 , with the structure from a layer of bulk ZrI_2 , black rectangle represents the new unit cell B) a layer of MX_3 , with a similar pattern representing bulk layers, for example $RuCl_3$ and CrI_3 with the $AlCl_3$ structure type; all atoms in the sketch are within one unit cell. Distances between the atoms are indicated as follows: the red dotted lines are the longest, followed by purple, blue, then mustard yellow. The distortions characteristic of ZrI_2 are much stronger than those of the MX_3 materials. The M site symmetries are C_{1h} for panel A and C_2 for panel B. No d-orbital degeneracies are enforced by either site symmetry.

C. Lower structural symmetries

Some of the dihalides and trihalides exhibit symmetries lower than trigonal. The point group C_{2h} , a subgroup of the trigonal point group D_{3d} , appears in both MX_2 and MX_3 compounds, namely in ZrI_2 , as well as in some polymorphs of $RuCl_3$ and CrI_3 . This symmetry reduction includes a breaking of the rotational symmetry, which splits the doublets, and may lead to minor mixing of the orbital eigenvalues; generally, subgroups of D_{3d} which do not maintain the 3-fold rotational symmetry lead to a breaking of the doublets' degeneracy.

Figure 5 shows that the single layers of ZrI_2 and $RuCl_3$ or CrI_3 no longer have three-fold rotational symmetry. The in-plane lattice parameters defining the formula unit of a di- or tri-halide lattice are no longer equivalent, and are replaced by perpendicular vectors describing the supercell that accommodates for this lower symmetry as described in the caption for the figure. This breaks the symmetry of the remaining two orbital doublet pairs. This symmetry reduction is associated with inequivalence of both the X-X bonds and the M-X bonds as indicated in Figure 5. In ZrI_2 this is plainly discerned as the bond distortions are sufficiently strong that the structures can be understood to form 1D zig-zag chains [52]. A minor mixing between the a_{1g} orbital and the other orbitals appears as a result of the symmetry lowering, and performing a Wannierization shows us that this minor mixing breaks its rotational symmetry.

The ZrI_2 structure also has additional forms of symmetry breaking beyond that leading to the C_{2h} point group; for example, the two layers that form the minimum structural unit are not completely equivalent. The octahedral

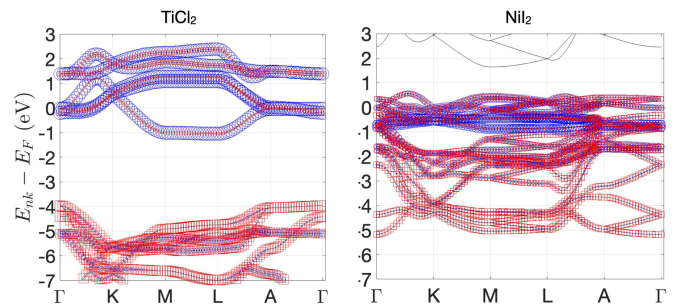


FIG. 6. DFT Band structure and Wannier ‘fat bands’ for a full $p-d$ model for (left) $TiCl_2$ and (right) NiI_2 , exemplifying materials that are in the Mott-Hubbard ($TiCl_2$) and charge-transfer (NiI_2) regimes. Blue circles correspond to transition metal M d state projections, red squares to ligand p states.

sizes differ between the layers. The symmetry of ZrI_2 is even lower in certain experimentally reported structures with two non-equivalent octahedra forming each layer leading to point group C_{2v} . Such further symmetry reductions are beyond the scope of this paper.

IV. ELECTRONIC CORRELATIONS AND LOCAL STRUCTURE EFFECTS

Many transition metal compounds exhibit correlated insulating states. The correlation physics that produces these states tends to favor high spin, filled and empty state configurations; the exact order is determined by a combination of correlation effects and electron-lattice coupling. Similar to perovskite oxides, 2D di- and tri-halides can be in the Mott-Hubbard or in the charge-transfer regime of the Zaanen-Sawatzky-Allen (ZSA) classification [53]. $TiCl_2$ is a clear example of a Mott-Hubbard material as the d and p states are clearly separated by 4 eV (Figure 6A). Similar to the transition metal perovskite case, going right along the periodic table, *i.e.*, towards higher orbital filling, the $p-d$ splitting decreases. In Figure 6B, we find the $p-d$ splitting is low for the well-known material NiI_2 [54–56] with the p and d bands overlapping in energy, corresponding to this insulating material being in the charge transfer regime.

A. Example of $TiCl_2$

We performed DFT + $U = 2$ eV calculations on the dihalide $TiCl_2$ in the experimental structure and allowing for spin symmetry breaking to gain initial insight into the role of correlations. The Hubbard on-site Coulomb interaction allows the opening of a gap in the electronic spectrum (≈ 0.375 eV), creating a fully orbital and spin polarized state (Figure 7 A). Taking the $TiCl_2$ experimental structure and allowing for spin-symmetry breaking, we find a high spin orbitally ordered state. The minority

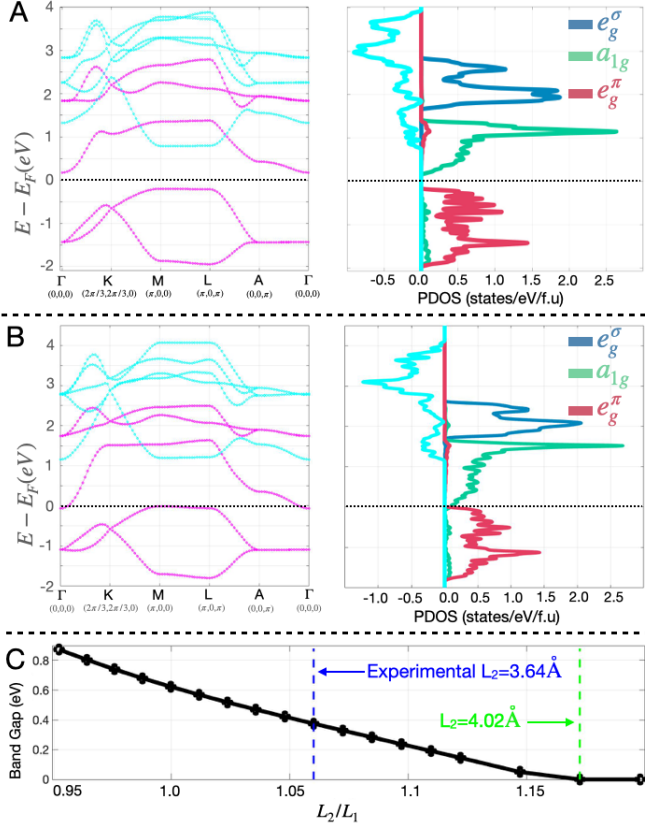


FIG. 7. Electronic band dispersions and orbital projected density of states for ferromagnetic, high-spin TiCl₂ at the DFT+ $U = 2$ eV level: (A) experimental structure and (B) structure with L_2 extended to 4.02 Å and inter-layer distance kept constant. Left: Bands, majority spin in magenta, minority spin in cyan. Right: projected density of states (PDOS), minority spin rescaled by dividing by 5. Increasing L_2/L_1 closes the gap by reducing the orbital polarization of the lower three orbitals. (C) Dependence of the electronic band gap in TiCl₂ with L_2/L_1 ratio for a fixed inter-layer distance.

spin channel is completely unoccupied. Two electrons reside in the majority spin channel of the two e_g^π orbitals, while the e_g^σ and a_{1g} occupations are essentially zero.

Calculations with structures obtained by elongating L_2 while keeping L_1 constant closes this gap, while shortening L_2 further opens the gap, by shifting the relative energy levels of the lowest three states (Figure 7). Similar effects can be obtained by changing the inter-layer distance as well. Importantly, we note that in the presence of electronic correlations, the electronic configuration favors the state that leads to fully occupied and empty states and the opening of a band gap, and a strong trigonal distortion is needed to counteract this effect. We note that, in a tetragonal basis, as discussed before, the lower three t_{2g} states would remain equivalent, as their lobes would point along equivalent directions, which would obscure the identity of the active orbitals – the singlet and doublet – participating in the band gap opening.

B. Survey of Broken Symmetry Phases

By varying the transition metal ion and considering both dihalides and trihalides, one can obtain all d^n configurations ranging from d^1 (TiI₃) to d^9 (CuCl₂, proposed below). As a result, a range of correlated insulating states can be produced, as shown in Figure 8. Some of these states will involve orbital order that breaks the trigonal symmetry, leading to the appearance of one dimensional lattice structures – or, more generally, structures that break the three-fold rotational symmetry.

In the d^1 configuration the natural Mott insulating state involves an electron in the a_{1g} orbital. This state preserves the trigonal symmetry. However the multiple superexchange pathways involving also the e_g^π orbitals suggest that unless L_2/L_1 can be made very small the ground state will be ferromagnetic. However if the L_2/L_1 ratio can be made large enough, a change in level ordering may occur and it is possible to have an orbitally ordered Mott insulator with one electron in the e_g^π orbitals and a corresponding orbital order and trigonal symmetry breaking lattice distortion.

In the d^2 case, we may generically expect a high spin ground state with two electrons in the e_g^π orbitals, as found in the DFT+ U calculations for TiCl₂. For a small enough L_2/L_1 ratio, however, a state with one electron in the a_{1g} orbital and one in e_g^π doublet may lift the trigonal symmetry.

The relatively smaller ligand field splitting in the halides relative to the octahedral perovskite oxides suggests that the d^4 , d^5 , d^6 state will all be high spin. The d^4 and d^6 configurations would also exhibit orbitally ordered and trigonally broken states; d^6 can also support an insulating diamagnetic state with the gap opened by the crystal field splitting between the 2 higher energy and lower 3 orbitals.

The d^7 state is most likely to be a $S = 1/2$ state with the lowest three orbitals fully occupied, and one of the e_g^σ orbitals half-filled and spin-polarized, likely leading to a structurally broken state of the form found in the materials with C_{2h} point symmetry. The d^8 configuration is most likely to be a $S = 1$ state with each e_g^σ orbital half-filled and spin-polarized. In some scenarios, it may be orbitally-polarized and non-magnetic, associated with a symmetry-breaking mode in the lattice, most likely as previously discussed.

Such configurations may be susceptible to metal-insulator transitions (MIT), which we assess using a recently devised machine-learning classification model [57]. We found that the binary MIT-non MIT classifier tends to predict most of the 2D halides are candidate MIT compounds, giving a positive MIT classification for CrCl₃, FeCl₃, IrBr₃, MnCl₂, RuCl₃, TiCl₂, VCl₃ and ZrI₂, and a negative classification for CrI₃, FeI₂ and NiI₂. This is likely due to the similarity of this class of materials to perovskite oxide MIT transition compounds, both in the structural features exhibited, such as the average transition metal-ligand distances which range between 2.4 Å

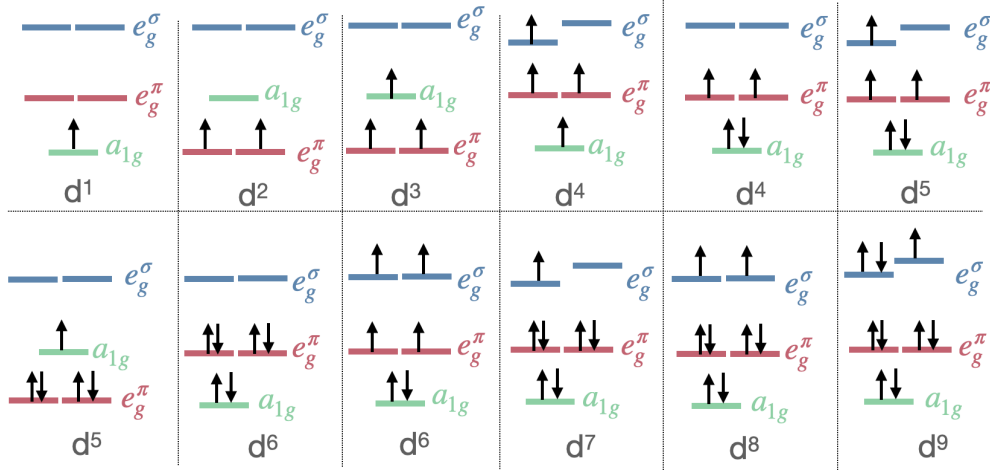


FIG. 8. Different possible electronic states for $d^1 - d^9$ occupations as discussed in the main text. Configurations that break the doublet degeneracy would be associated with further lattice distortions, reducing symmetry below trigonal. States with higher a_{1g}/e_g^π occupation ratios are likely to have a higher L_2/L_1 ligand bond ratio.

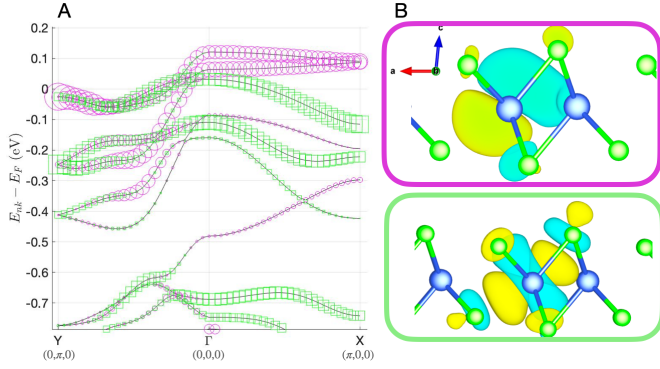


FIG. 9. A) DFT band structure, and 'fat bands' of the top two Wannier orbitals on the hypothetical CuCl_2 monolayer discussed in the main text. B) Real-space isosurfaces of the highest energy d-orbitals, with occupations 0.912 and 0.93 per spin channel. Due to the pseudo-1D nature of the symmetry broken lattice structure, there is relatively little dispersion along the Γ -X direction.

and 3.01 \AA , the metal-metal distances of $3.3\text{--}4.2 \text{ \AA}$, and electronic descriptors, e.g., estimated unscreened Hubbard U values. However, due to their intrinsic broken symmetry and reduced dimensionality, these materials generally will be exclusively insulating. Similar to MIT compounds, the 2D halides will tend to display coupled electronic and lattice transitions at low temperatures [30].

For the d^9 and possibly d^4 configurations, the presence of one hole in the e_g^σ manifold implies a breaking of rotational symmetry and likely, a one dimensional electronic structure. To examine this possibility, we perform the following simulation. We take a single layer of the experimental ZrI_2 structure and replace Zr with Cu and I with Cl without allowing the structure to relax. Owing to the strong charge-transfer character of the resulting

theoretical material, the Cu d manifold is mostly filled. Nonetheless, after performing the appropriate rotation of the d -shell basis, we find that the two least-occupied orbitals are e_g^σ like (Figure 9). These orbitals display non-zero orbital polarization with one orbital with $d_{x^2-y^2}$ character pointing along Cu-Cl bonds along the 1D chain, and one orbital of $d_{3z^2-r^2}$ character pointing towards Cu-Cl bonds that connect the 1D chains. This type of symmetry breaking can likely be exploited, provided the appropriate material strains, to form 1D conducting chains out of a 2D structure. This behavior is similar to how the pseudo-2D electronic structure of cuprate-like high-temperature superconductors forms from out of 3D conducting building blocks. Another orbitally polarized state can also be obtained with a different orbital basis for the d^9 configuration [58].

V. CONCLUSIONS

We showed that the highest possible metal orbital symmetry of 2D dihalides and trihalides comprising edge-shared MX_6 octahedra is trigonal, and analysed the interplay of atomic lattice, orbital physics and correlation effects. Within this trigonal basis, we showed that the amplitude of the electronic orbital splittings can be tuned by both the interlayer distance, as well as through changing the ligand-ligand bond ratio L_2/L_1 , and that the effect of correlations strongly favors ordered states.

In addition, the orbital occupancies can be sensitively tuned through changes in these atomic structure features, which can be achieved experimentally via pressure, strain, as well as possibly via optical excitations of the relevant structural modes to enable control of magnetic configurations and other electronic ordering. We showed that these materials can be analyzed from the point of view of the ZSA classification.

We showed how one can build and analyze a Wannier model corresponding to this reduced symmetry, symmetry which can lead to novel (correlated) electronic states. Our work serves as a basis to understand correlated phenomena in this class of materials, and their interplay with lattice symmetry modes, and easily allows for models to disentangle their roles - similar to recently built models on perovskites and their Ruddlesden-Popper phases [11, 17, 59, 60]. Our results may be particularly important in the search for candidate spin-liquids. Spin liquid states are predicted to be found in the vicinity of a Mott transition and in symmetric highly-frustrated structures. Our generic finding of strong orbital ordering and associated trigonal symmetry breaking will be important in appropriately modeling - and discovering - potential spin liquids and other novel states.

ACKNOWLEDGMENTS

This research was supported in part by the National Science Foundation (NSF) under DMREF Award DMR-

1729303. The information, data, or work presented herein was funded in part by the Advanced Research Projects Agency-Energy (ARPA-E), U.S. Department of Energy, under Award Number DE-AR0001209. AJM is supported in part by Programmable Quantum Materials, an Energy Frontier Research Center funded by the U.S. Department of Energy (DOE), Office of Science, Basic Energy Sciences (BES), under award DE-SC0019443. The views and opinions of authors expressed herein do not necessarily state or reflect those of the United States Government or any agency thereof. The Flatiron Institute is a division of the Simons Foundation.

-
- [1] D. G. Schlom, L. Q. Chen, C. B. Eom, K. M. Rabe, S. K. Streiffer, and J. M. Triscone, *Annual Review of Materials Research* **37**, 589 (2007).
 - [2] V. Garcia, M. Bibes, L. Bocher, S. Valencia, F. Kronast, A. Crassous, X. Moya, S. Enouz-Vedrenne, A. Gloter, D. Imhoff, C. Deranlot, N. Mathur, S. Fusil, K. Bouzehouane, and A. Barthelémy, *Science* **327**, 1106 (2010).
 - [3] Y. Qi and K. M. Rabe, <http://arxiv.org/abs/2103.16466> (2021).
 - [4] H. Chen, Q. Qiao, M. S. J. Marshall, A. B. Georgescu, A. Gulec, P. J. Phillips, R. F. Klie, F. J. Walker, and C. H. Ahn, *Nano. Lett* **14**, 4965 (2014).
 - [5] Y. Tokura, *Current Opinion in Solid State and Materials Science* **3**, 175 (1998).
 - [6] M. Gibertini, M. Koperski, A. F. Morpurgo, and K. S. Novoselov, *Nature Nanotechnology* **14**, 408 (2019).
 - [7] S. Koohfar, A. B. Georgescu, A. N. Penn, J. M. LeBeau, E. Arenholz, and D. P. Kumah, *npj Quantum Materials* **4**, 25 (2019).
 - [8] H. J. A. Molegraaf, J. Hoffman, C. A. F. Vaz, S. Gariglio, D. Van Der Morel, C. H. Ahn, and J. M. Triscone, *Advanced Materials* **21**, 1 (2009).
 - [9] Y. Mizuguchi, F. Tomioka, S. Tsuda, T. Yamaguchi, and Y. Takano, *Applied Physics Letters* **93**, 152505 (2008).
 - [10] S. Koohfar, A. B. Georgescu, I. Hallsteinsen, R. Sachan, M. A. Roldan, E. Arenholz, and D. P. Kumah, *Physical Review B* **101**, 064420 (2020).
 - [11] A. Georgescu and A. J. Millis, <http://arxiv.org/abs/2105.02271> (2021).
 - [12] G. G. Guzmán-Verri, R. T. Brierley, and P. B. Littlewood, *Nature* **576**, 429 (2019).
 - [13] J. Shamblyn, M. Heres, H. Zhou, J. Sangoro, M. Lang, J. Neuefeind, J. A. Alonso, and S. Johnston, *Nature Communications* **9**, 86 (2018).
 - [14] P. Zubko, S. Gariglio, M. Gabay, P. Ghosez, and J.-m. Triscone, *Annual Review of Condensed Matter Physics* , 141 (2011).
 - [15] M. Forst, A. D. Caviglia, R. Scherwitsl, R. Mankowsky, P. Zubko, V. Khanna, H. Bromberger, S. B. Wilkins, Y. D. Chuang, W. S. Lee, W. F. Schlotter, J. J. Turner, G. L. Dakovski, M. P. Minitti, J. Robinson, S. R. Clark, D. Jaksch, J. M. Triscone, J. P. Hill, S. S. Dhesi, and A. Cavalleri, *Nature Materials* **14**, 883 (2015).
 - [16] M. Medarde, P. Lacorre, K. Conder, F. Fauth, and A. Furber, *Physical Review Letters* **80**, 2397 (1998).
 - [17] A. B. Georgescu, O. E. Peil, A. S. Disa, A. Georges, and A. J. Millis, *Proceedings of the National Academy of Sciences of the United States of America* **116**, 14434 (2019).
 - [18] C. Domínguez, A. B. Georgescu, B. Mundet, Y. Zhang, J. Fowlie, A. Mercy, A. Waelchli, S. Catalano, D. T. Alexander, P. Ghosez, A. Georges, A. J. Millis, M. Gibert, and J. M. Triscone, *Nature Materials* **19**, 1182 (2020).
 - [19] D. Lee, B. Chung, Y. Shi, N. Campbell, F. Xue, K. Song, J. P. Podkaminer, T. H. Kim, P. J. Ryan, T. R. Paudel, J. W. Spinuzzi, D. A. Tenne, E. Y. Tsymbal, M. S. Rzchowski, L. Q. Chen, J. Lee, and C. B. Eom, *Science* , 1037 (2018).
 - [20] A. D. Caviglia, M. Först, R. Scherwitsl, V. Khanna, H. Bromberger, R. Mankowsky, R. Singla, Y. D. Chuang, W. S. Lee, O. Krupin, W. F. Schlotter, J. J. Turner, G. L. Dakovski, M. P. Minitti, J. Robinson, V. Scagnoli, S. B. Wilkins, S. A. Cavill, M. Gibert, S. Gariglio, P. Zubko, J. M. Triscone, J. P. Hill, S. S. Dhesi, and A. Cavalleri, *Physical Review B - Condensed Matter and Materials Physics* **88**, 220401(R) (2013).
 - [21] N. J. Szymanski, L. N. Walters, D. Puggioni, and J. M. Rondinelli, *Physical Review Letters* , 236402 (2019).
 - [22] J. H. Chu, H. Kue, J. Analytis, and I. Fisher, *Science* **337**, 710 (2012).

- [23] P. A. Lee, N. Nagaosa, and X. G. Wen, *Reviews of Modern Physics* **78**, 17 (2006).
- [24] M. R. Norman, *Physics* **13**, 10.1103/physics.13.85 (2020).
- [25] S. Gariglio, N. Reyren, A. D. Caviglia, and J. M. Triscone, *Journal of Physics Condensed Matter* **21**, 164213 (2009).
- [26] B. Keimer, S. A. Kivelson, M. R. Norman, S. Uchida, and J. Zaanen, *Nature* **518**, 179 (2015).
- [27] C. Huang, F. Wu, S. Yu, P. Jena, and E. Kan, *Physical Chemistry Chemical Physics* **22**, 512 (2020).
- [28] S. Son, M. J. Coak, N. Lee, J. Kim, T. Y. Kim, H. Hamidov, H. Cho, C. Liu, D. M. Jarvis, P. A. Brown, J. H. Kim, C. H. Park, D. I. Khomskii, S. S. Saxena, and J. G. Park, *Physical Review B* **99**, 041402(R) (2019).
- [29] S. Tian, J. F. Zhang, C. Li, T. Ying, S. Li, X. Zhang, K. Liu, and H. Lei, *Journal of the American Chemical Society* **141**, 5326 (2019).
- [30] E. Gati, Y. Inagaki, T. Kong, R. J. Cava, Y. Furukawa, P. C. Canfield, and S. L. Bud'ko, *Physical Review B* **100**, 94408 (2019).
- [31] B. Lyu, Y. Gao, Y. Zhang, L. Wang, X. Wu, Y. Chen, J. Zhang, G. Li, Q. Huang, N. Zhang, Y. Chen, J. Mei, H. Yan, Y. Zhao, L. Huang, and M. Huang, *Nano Letters* **20**, 6024 (2020).
- [32] M. An, Y. Zhang, J. Chen, H. M. Zhang, Y. Guo, and S. Dong, *Journal of Physical Chemistry C* **123**, 30545 (2019).
- [33] R. Yadav, N. A. Bogdanov, V. M. Katukuri, S. Nishimoto, J. Van Den Brink, and L. Hozoi, *Scientific Reports* **6**, 1 (2016).
- [34] T. Yokoi, S. Ma, Y. Kasahara, S. Kasahara, T. Shibauchi, N. Kurita, H. Tanaka, J. Nasu, Y. Motome, C. Hickey, S. Trebst, and Y. Matsuda, *Science* **373**, 568 (2021).
- [35] H. Suzuki, H. Liu, J. Bertinshaw, K. Ueda, H. Kim, S. Laha, D. Weber, Z. Yang, L. Wang, H. Takahashi, K. Fürsich, M. Minola, B. V. Lotsch, B. J. Kim, H. Yavaş, M. Daghofer, J. Chaloupka, G. Khaliullin, H. Gretarsson, and B. Keimer, *Nature Communications* **12**, 1 (2021).
- [36] H. Li, T. T. Zhang, A. Said, G. Fabbris, D. G. Mazzone, J. Q. Yan, D. Mandrus, G. B. Halász, S. Okamoto, S. Murakami, M. P. Dean, H. N. Lee, and H. Miao, *Nature Communications* **12**, 4 (2021).
- [37] H. Takagi, T. Takayama, G. Jackeli, G. Khaliullin, and S. E. Nagler, *Nature Reviews Physics* **1**, 264 (2019).
- [38] M. Hermanns, I. Kimchi, and J. Knolle, *Annual Review of Condensed Matter Physics* **9**, 17 (2018).
- [39] M. Blei, J. L. Lado, Q. Song, D. Dey, O. Erten, V. Pardo, R. Comin, S. Tongay, and A. S. Botana, *Applied Physics Reviews* **8**, 10.1063/5.0025658 (2021).
- [40] D. Wang and B. Sanyal, *Journal of Physical Chemistry C* **125**, 18467 (2021).
- [41] T. Kong, S. Guo, D. Ni, and R. J. Cava, *Physical Review Materials* **3**, 084419 (2019).
- [42] X. Chen, X. Fan, L. Li, N. Zhang, Z. Niu, T. Guo, S. Xu, H. Xu, D. Wang, H. Zhang, A. S. McLeod, Z. Luo, Q. Lu, A. J. Millis, D. N. Basov, M. Liu, and C. Zeng, *Nature Physics* **16**, 631 (2020).
- [43] G. F. Dionne, in *Magnetic Oxides* (Springer US, Boston, MA, 2009) pp. 37–106.
- [44] M. A. McGuire, *Crystals* **7**, 10.3390/cryst7050121 (2017).
- [45] A. S. Botana and M. R. Norman, *Physical Review Materials* **3**, 044001 (2019).
- [46] M. Hellenbrandt, *Crystallogr. Rev.* **10**, 17 (2004).
- [47] S. V. Streltsov and D. I. Khomskii, *Physics-Uspekhi* **60**, 1121 (2017).
- [48] N. Wagner, R. Seshadri, and J. M. Rondinelli, *Phys. Rev. B* **100**, 064101 (2019).
- [49] Note that for the cubic case, the conventional coordinate system involves a z axis chosen parallel to an M-X bond while for the trigonal case the conventional coordinate system involves a z axis passing through an octahedral face (*i.e.*, along [111] in conventional octahedral coordinates).
- [50] DFT calculations were performed using the Quantum Espresso software package on a 3 atom formula unit, using ultrasoft pseudopotentials using the PBE exchange-correlation functional, an energy cutoff of 748eV and a 20x20x20 k-grid. Orbital occupations were obtained using the orthonormal atomic projections, as implemented in Quantum Espresso; DFT+U calculations were performed with the U applied to orthonormal atomic projections as well, within the Dudarev simplified +U formalism.
- [51] A. A. Mostofi, J. R. Yates, G. Pizzi, Y. S. Lee, I. Souza, D. Vanderbilt, and N. Marzari, *Computer Physics Communications* **185**, 2309 (2014).
- [52] D. H. Guthrie and J. D. Corbett, *Journal of Solid State Chemistry* **37**, 256 (1981).
- [53] J. Zaanen, G. A. Sawatzky, and J. W. Allen, *Physical Review Letters* **55**, 418 (1985).
- [54] C. R. Ronda, G. J. Arends, and C. Haas, *Physical Review B* **35**, 4038 (1987).
- [55] H. Starnberg, M. Johnson, and H. Hughes, *Journal of Physics C: Solid State Physics* **19**, 2689 (1986).
- [56] G. Van Der Laan, J. Zaanen, G. A. Sawatzky, R. Karnatak, and J. M. Esteva, *Physical Review B* **33**, 4253 (1986).
- [57] A. B. Georgescu, P. Ren, A. R. Toland, S. Zhang, K. D. Miller, D. W. Apley, E. A. Olivetti, N. Wagner, and J. M. Rondinelli, *Chemistry of Materials* **33**, 5591 (2021).
- [58] H. Qin, J. Chen, B. Sun, Y. Tang, Y. Ni, Z. Chen, H. Wang, and Y. Chen, *Physical Chemistry Chemical Physics*, 22078 (2021).
- [59] O. E. Peil, A. Hampel, C. Ederer, and A. Georges, *Physical Review B* **99**, 245127 (2019).
- [60] Q. Han and A. Millis, *Physical Review Letters* **121**, 67601 (2018).